Supporting Information

Sulfone-Rhodamines: A New Class of Near-Infrared Fluorescent Dyes for Bioimaging

*Jing Liu, Yuan-Qiang Sun, Hongxing Zhang, Heping Shi, Yawei Shi, and Wei Guo**

†School of Chemistry and Chemical Engineering and ‡Institute of Biotechnology, Shanxi University, Taiyuan 030006, China.

***Corresponding Author:** E-mail: guow@sxu.edu.cn

1. Supplementary Spectra

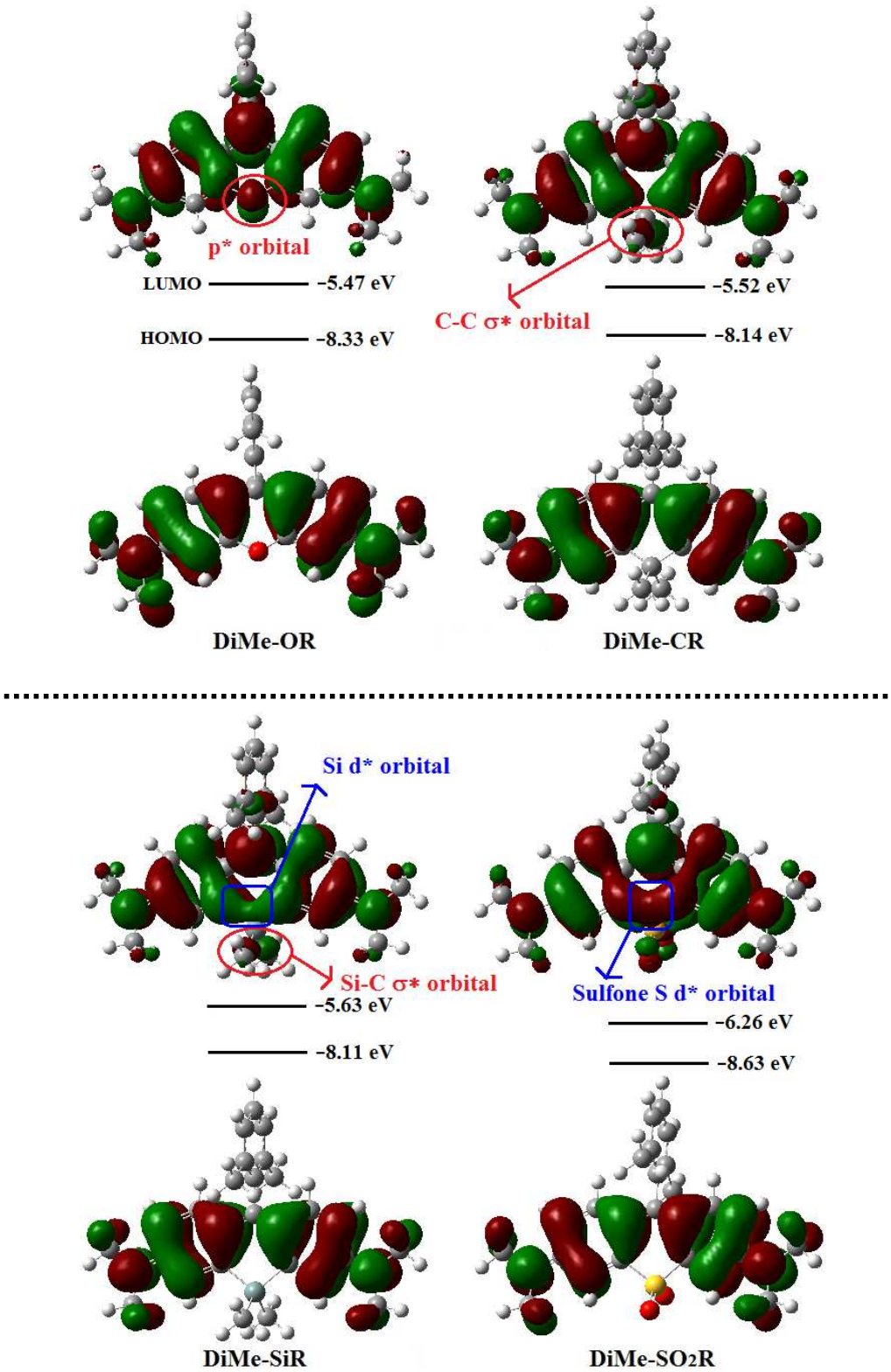

Figure S1. The frontier orbitals and energy levels of **DiMe-OR**, **DiMe-CR**, **DiMe-MG**, **DiMe-SiR**, and **DiMe-SO$_2$R**, calculated by DFT at the B3LYP/6-31+G(d,p) level of Gaussian

09. Ellipse regions show the p* orbital of O atom and σ* orbitals of C–C or Si–C bond, all of which are in anti-phase with adjacent π* orbital, indicating a repulsive interaction between them as well as the destabilizing effect of p*–π* and σ*–π* conjugations on LUMOs of **DiMe-OR**, **DiMe-CR** or **DiMe-SiR**. Rectangular regions show the *d**–π* conjugation between the *d**-orbital of Si or S atom (in sulfone group) with adjacent π* orbital, where the *d**-orbital is in in-phase with π* orbital, indicating the stabilizing effect of *d**–π* conjugation on LUMOs of **DiMe-SiR** and **DiMe-SO_2R**.

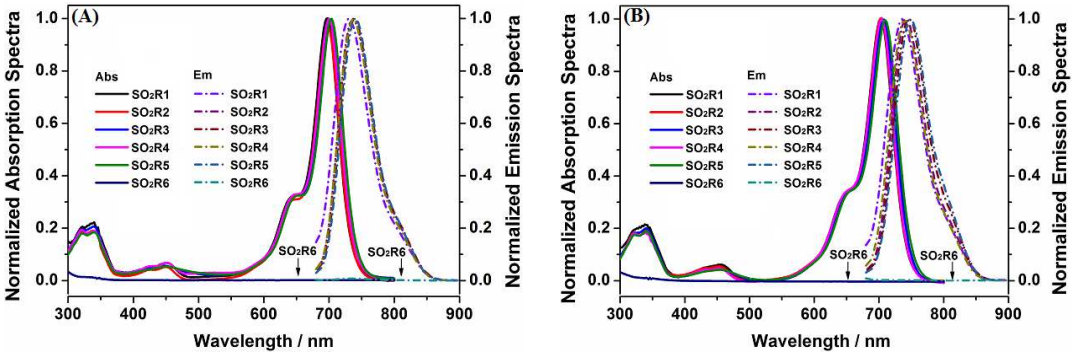

Figure S2. Normalized absorption and emission spectra of **SO_2R1–6** in CH_3CN (A) and PBS (20 mM, pH = 7.4, containing 0.25% CH_3CN) (B) at 25 ^oC. λ_{ex} = 660 nm; Slits: 10/10 nm; voltage: 600 V.

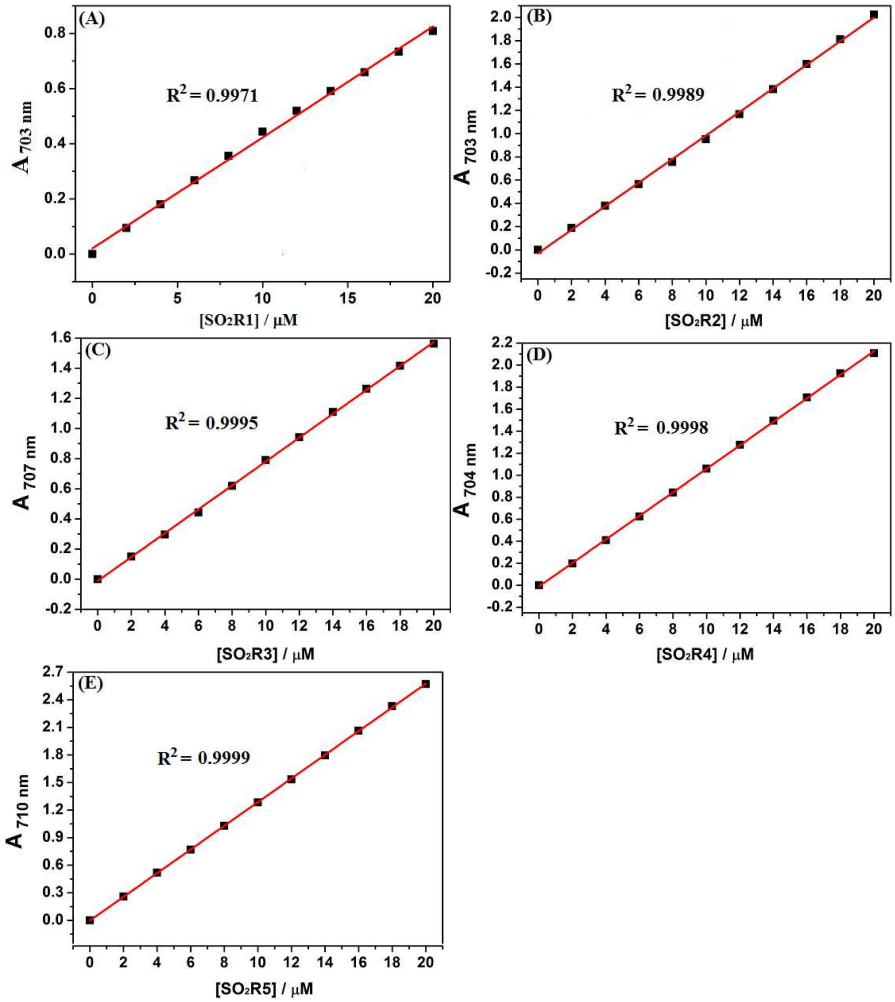

Figure S3. Solubility evaluation of **SO_2R1–5** in PBS (20 mM, pH = 7.4) by absorption spectra. (A-E) Plots of absorption intensity *vs* dye concentrations for **SO_2R1–5**, respectively.

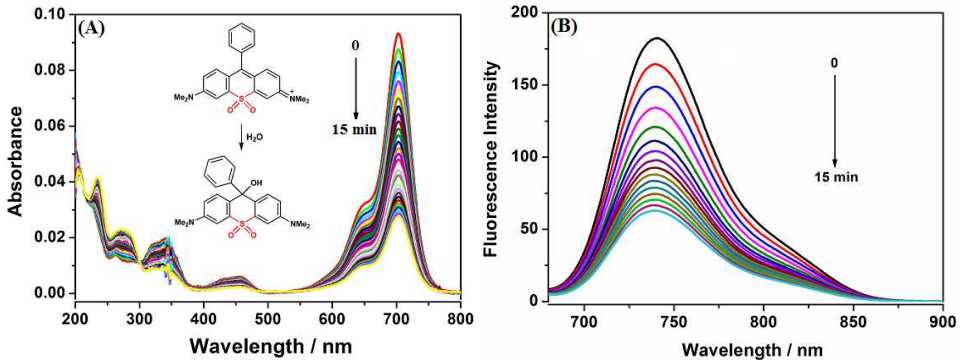

Figure S4. Time-dependent absorption (A) and fluorescence spectra (B) changes of **SO_2R1** (2.0 μM) in PBS (20 mM, pH = 7.4). The data indicates that **SO_2R1** is water unstable due to the nucleophilic attack of water molecule toward its electron-deficient and less steric 9-position that results in the disruption of its π-conjugation system (Inset in A).

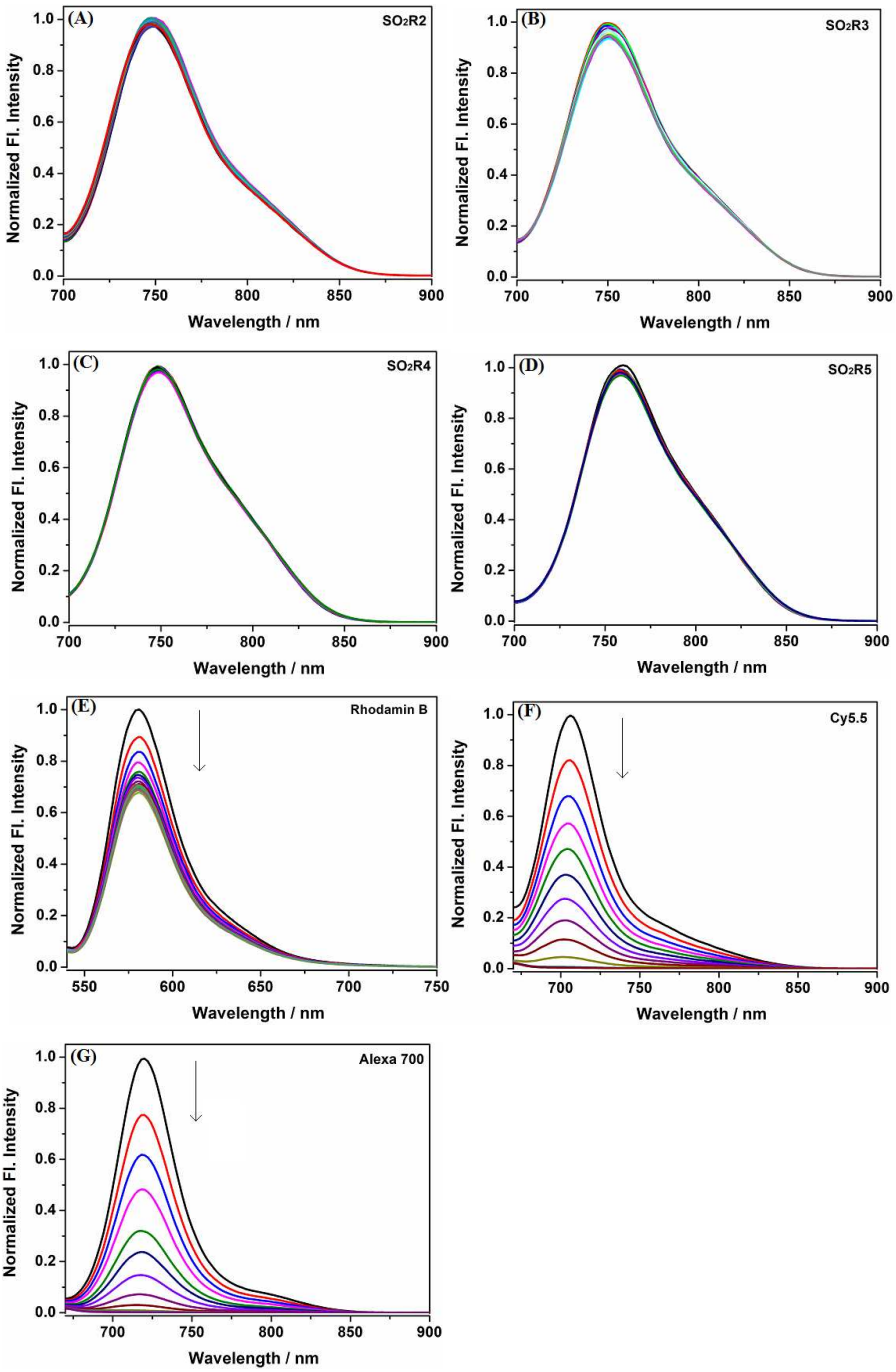

Figure S5. Normalized time-dependent fluorescence spectra of **SO_2R2–5** (A-D), rhodamine B (E), Cy5.5 (F), and Alexa700 (G) in PBS (20 mM, pH = 7.4) under continuous irradiation by a 300 W Xe lamp for 30 min. These data correspond with those shown in Figure 3A in the text.

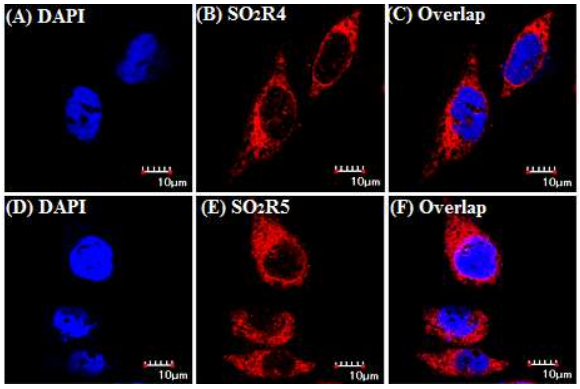

Figure S6. Fluorescence confocal images of HeLa cells costained with **SO_2R4** (or **SO_2R5**) (5 μM, 10 min) and nuclei dye DAPI (1 μg/mL, 10 min) at 37 ^{o}C in DMEM medium. (A–C) HeLa cells costained with **SO_2R4** and DAPI. (D–F) HeLa cells costained with **SO_2R4** and DAPI. For **SO_2R4** (or **SO_2R5**), emission was collected at 680–780 nm (λ_{ex}: 633 nm). For DAPI, emission was collected at 425–525 nm (λ_{ex}: 405 nm). Scale bar: 10 μm.

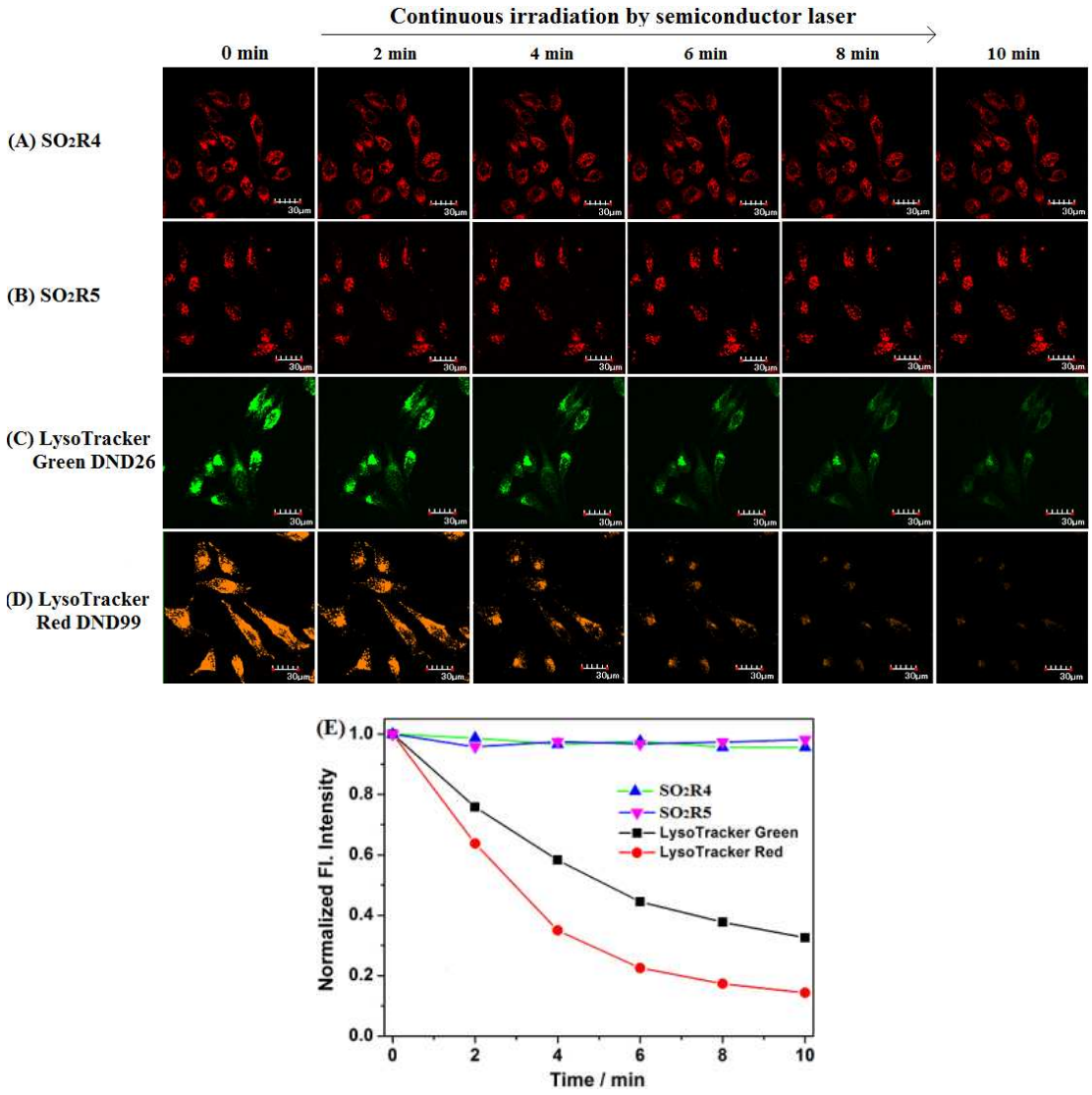

Figure S7. The intracellular photostability assays. (A–D) Time-dependent confocal images of HeLa cells stained with **SO_2R4**, **SO_2R5**, LysoTracker Red DND-99, and LysoTracker Green DND-26, respectively, in DMEM medium under continuous irradiation by semiconductor laser (633 nm for **SO_2R4** and **SO_2R5**; 559 nm for LysoTracker Red DND-99; 488 nm for LysoTracker Green DND-26, voltage: 800 V) for 10 min. Images were obtained at indicated time point. Scale bar: 30 μm. (E) The corresponding time-dependent fluorescence intensity changes in (A–D).

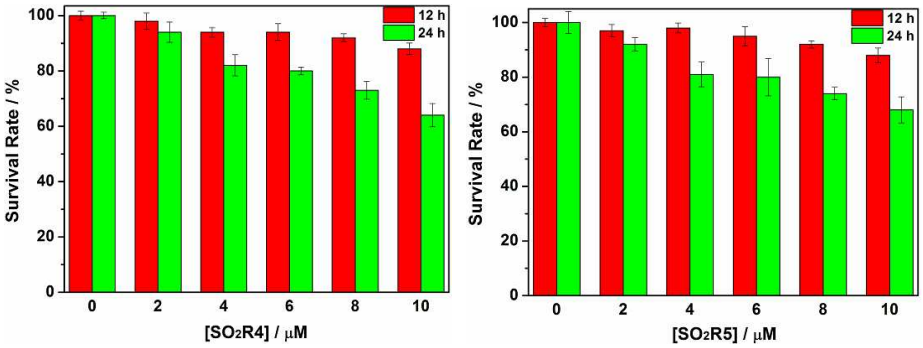

Figure S8. Percentage of viable Coca-2 cells after treatment with increasing concentrations of **SO_2R4** and **SO_2R5** after 12 h and 24 h, respectively.

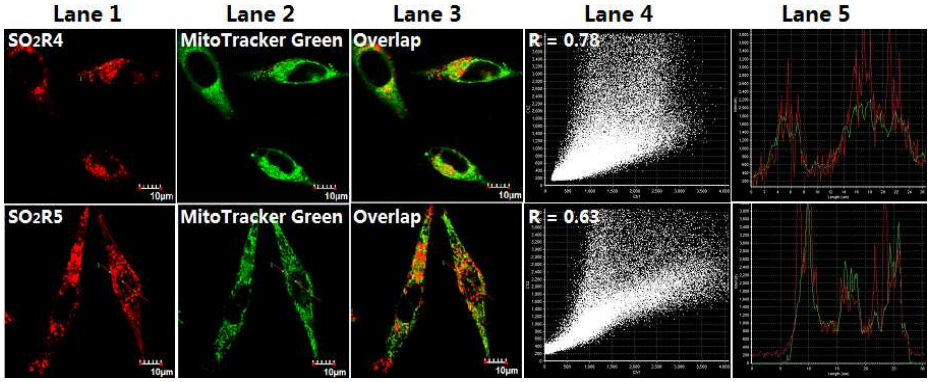

Figure S9. Fluorescence confocal images of HeLa cells stained with **SO_2R4** or **SO_2R5** (5 μM, 10 min) and then MitoTracker green FM (0.5 μM, 10 min) at 37 ^{o}C in DMEM medium. Lane 1: images of **SO_2R4** and **SO_2R5**; Lane 2: images of MitoTracker green FM; Lane 3: overlap images of Lane 1 and Lane 2; Lane 4: co-localization scatter plots and Pearson's co-localization coefficients; Lane 5: intensity profile of regions of interest (ROI) across HeLa cells. For Lane 1, emission was collected at 680–780 nm (λ_{ex}: 633 nm). For Lane 2, emission was collected at 500–600 nm (λ_{ex}: 488 nm). Scale bar: 10 μm.

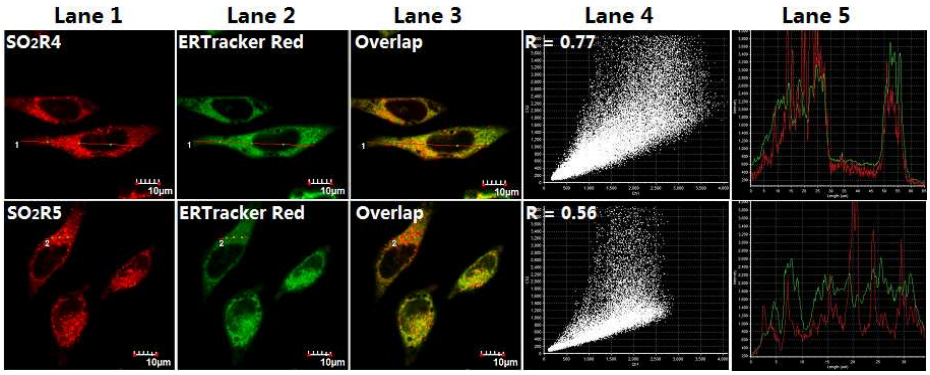

Figure S10. Fluorescence confocal images of HeLa cells stained with **SO_2R4** or **SO_2R5** (5 μM, 10 min) and then ERTracker™ Red (0.5 μM, 10 min) at 37 °C in DMEM medium. Lane 1: images of **SO_2R4** and **SO_2R5**; Lane 2: pseudo-colored images of ERTracker™ Red; Lane 3: overlap images of Lane 1 and Lane 2; Lane 4: co-localization scatter plots and Pearson's co-localization coefficients; Lane 5: intensity profile of regions of interest (ROI) across HeLa cells. For Lane 1, emission was collected at 680–780 nm (λ_{ex}: 633 nm). For Lane 2, emission was collected at 570–625 nm (λ_{ex}: 559 nm). Scale bar: 10 μm.

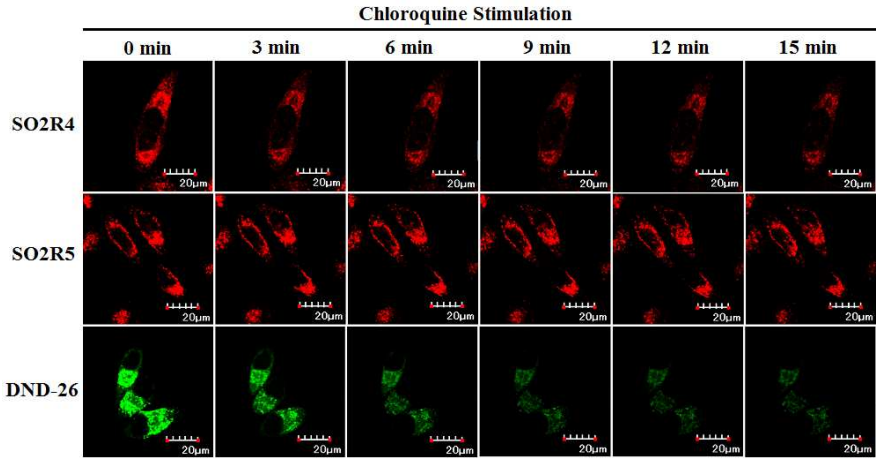

Figure S11. Fluorescence images of HeLa cells stained with **SO2R4** (5 μM), **SO2R5** (5 μM), and LysoTracker Green DND-26 (0.5 μM), respectively, after chloroquine (10 μM) stimulation for 0, 3, 6, 9, 12, and 15 min. Chloroquine, which can cause the leakage of protons out of lysosomes, is used to increase lysosomal pH.[1,2] These results reveal that **SO_2R5** has more stable lysosome localization and stable fluorescence against chloroquine-induced lysosome lysosomal pH increase.

2. ^{1}H NMR, ^{13}C NMR and HRMS charts of SO_2R1-6 and intermediates 2 and 3.

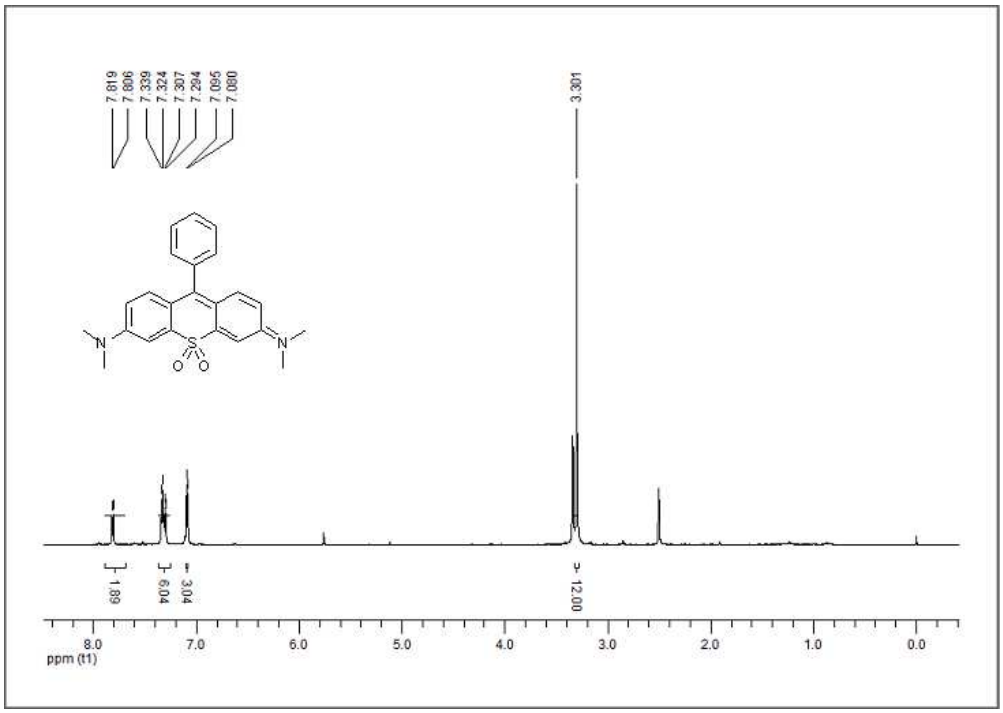

Figure S12. ^{1}H NMR chart of **SO_2R1** (DMSO-d_6, 600 MHz).

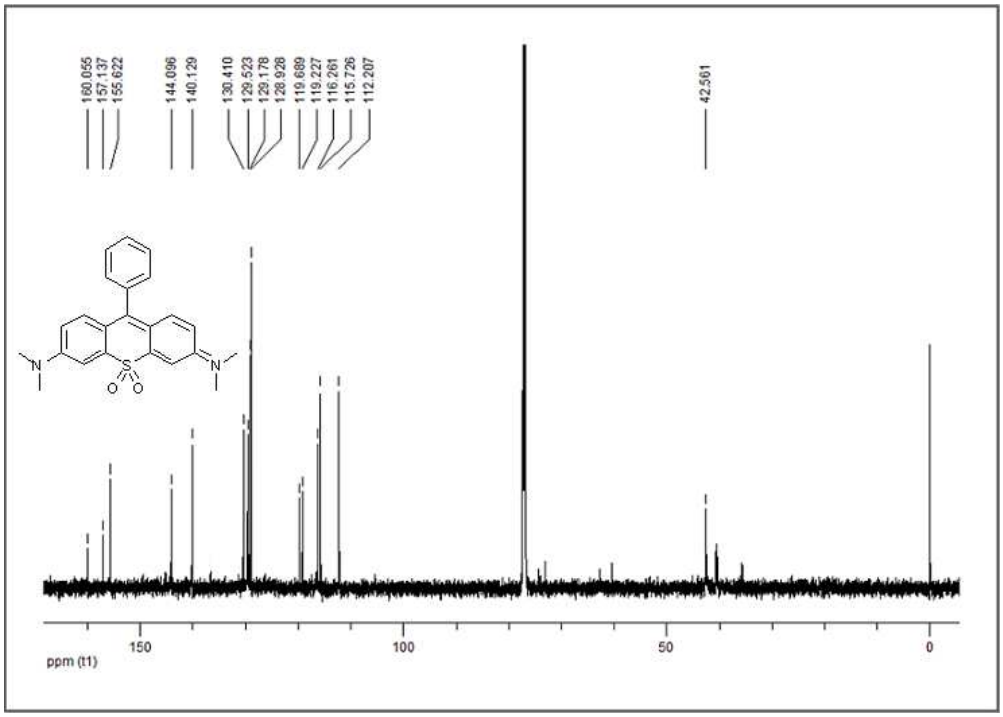

Figure S13. ^{13}C NMR chart of **SO_2R1** ($CDCl_3$, 150 MHz).

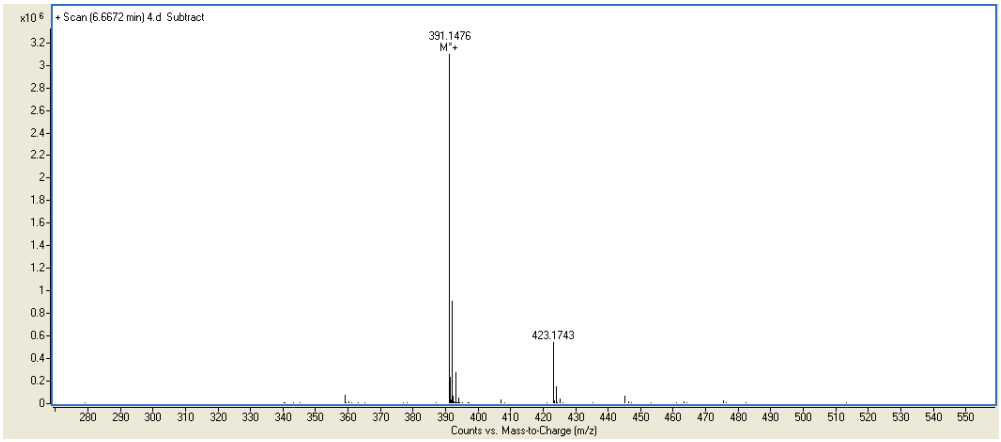

Figure S14. HRMS chart of **SO_2R1**.

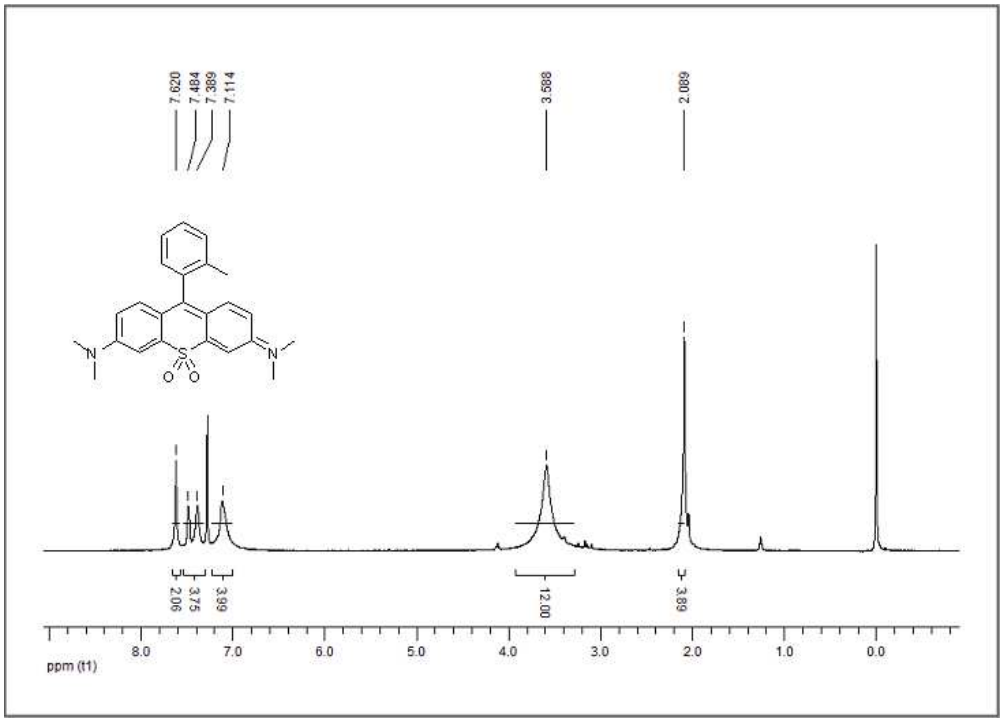

Figure S15. ^{1}H NMR chart of **SO_2R2** ($CDCl_3$, 600 MHz).

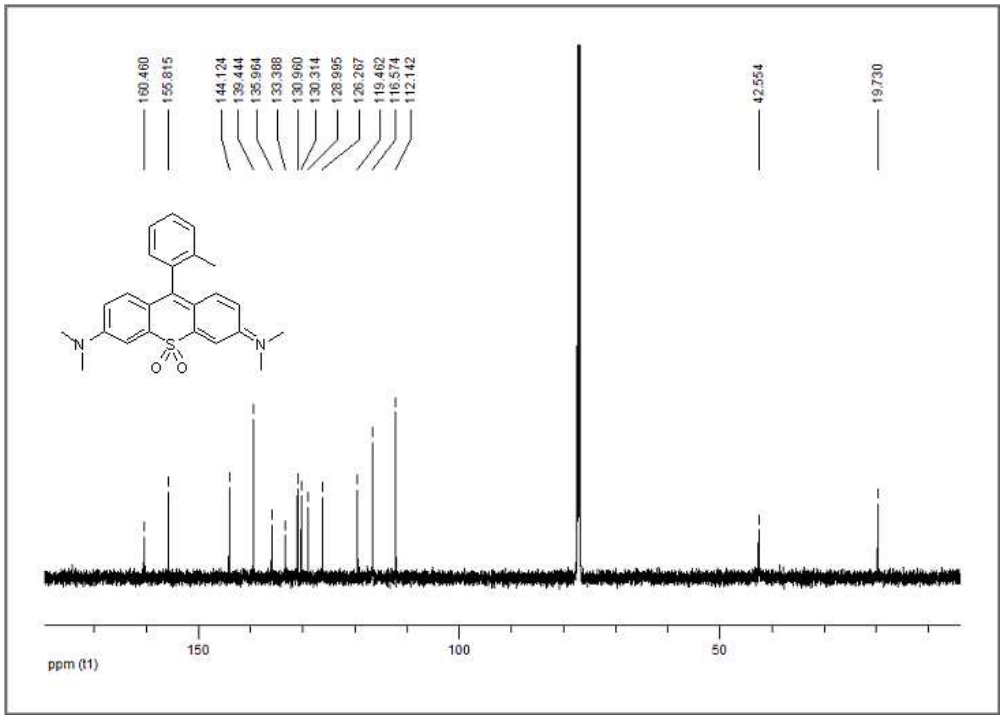

Figure S16. ^{13}C NMR chart of **SO_2R2** ($CDCl_3$, 150 MHz).

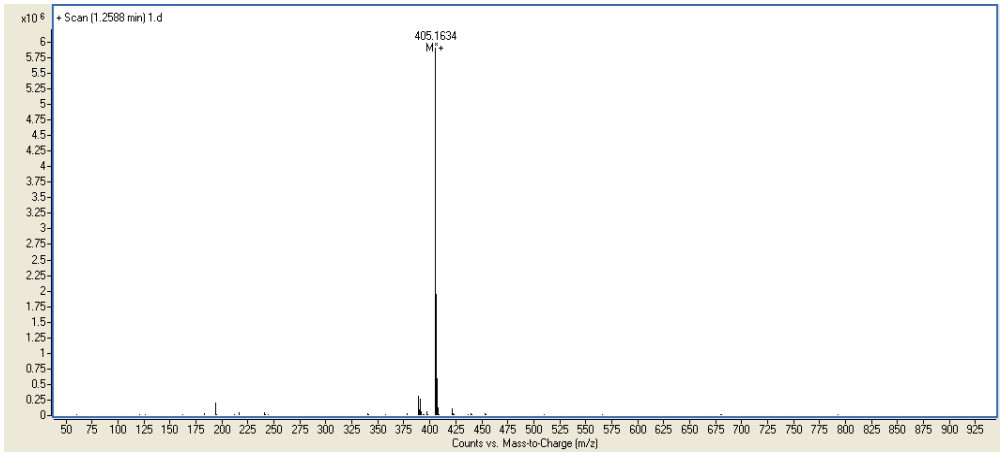

Figure S17. HRMS chart of **SO_2R2**.

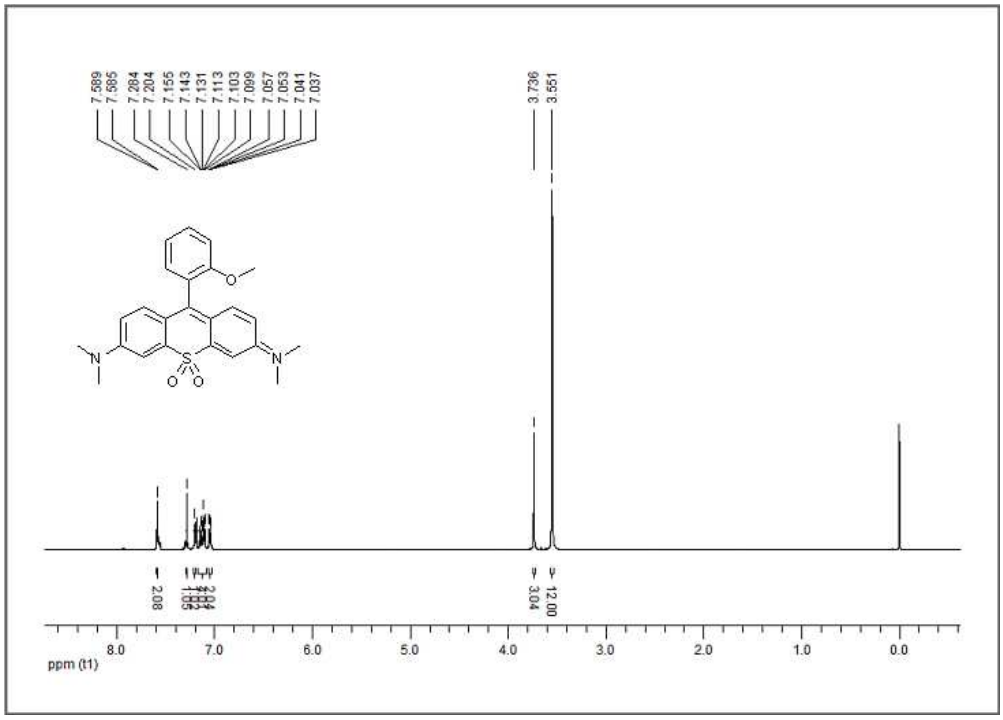

Figure S18. ^{1}H NMR chart of **SO_2R3** ($CDCl_3$, 600 MHz).

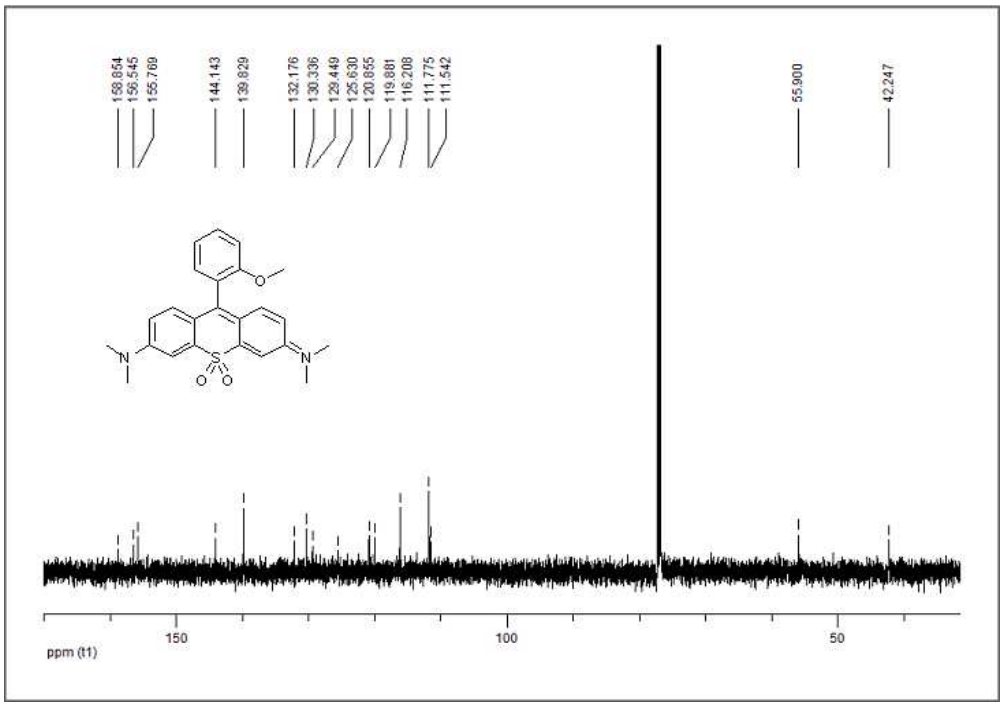

Figure S19. ^{13}C NMR chart of **SO_2R3** ($CDCl_3$, 150 MHz).

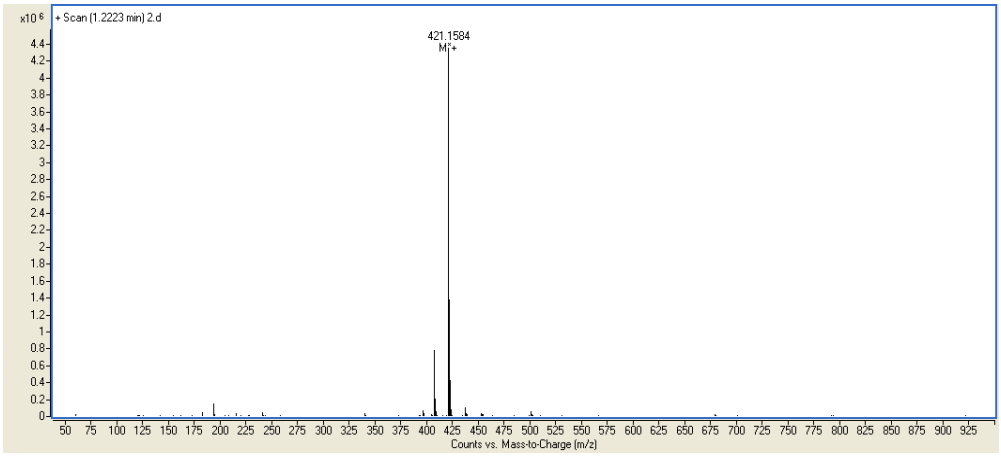

Figure S20. HRMS chart of **SO_2R3**.

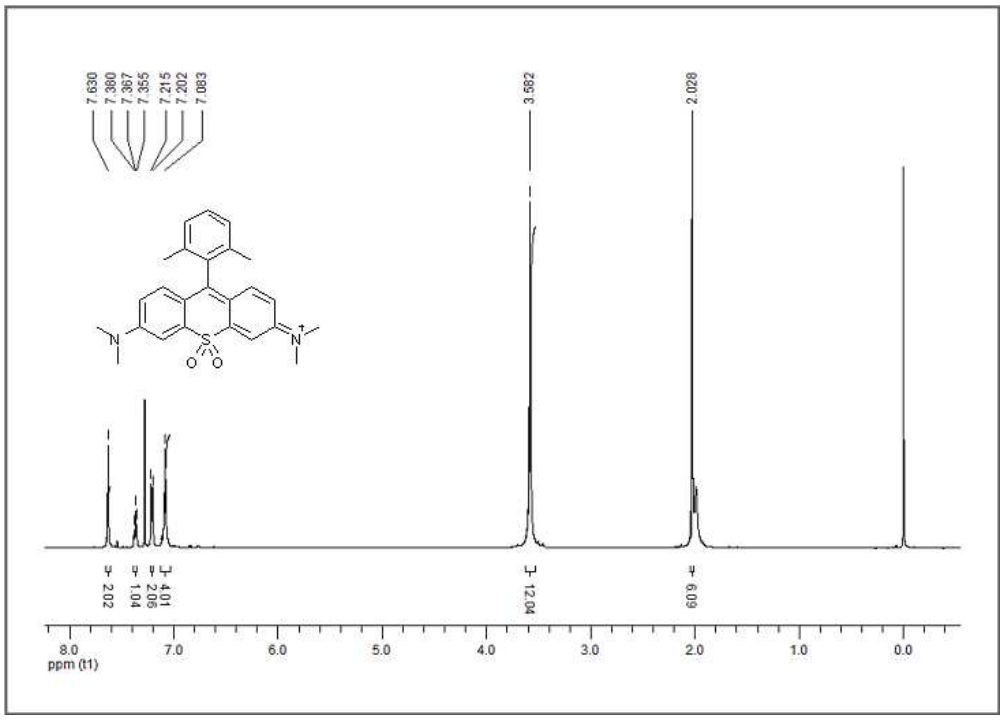

Figure S21. ^{1}H NMR chart of **SO_2R4** ($CDCl_3$, 600 MHz).

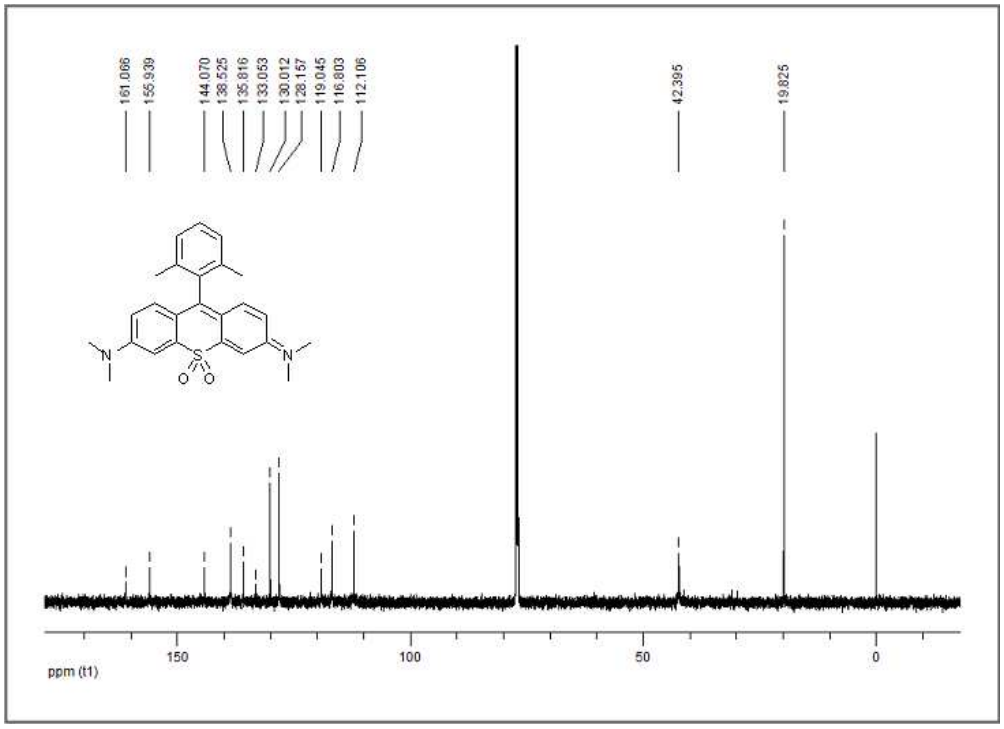

Figure S22. ^{13}C NMR chart of **SO_2R4** ($CDCl_3$, 150 MHz).

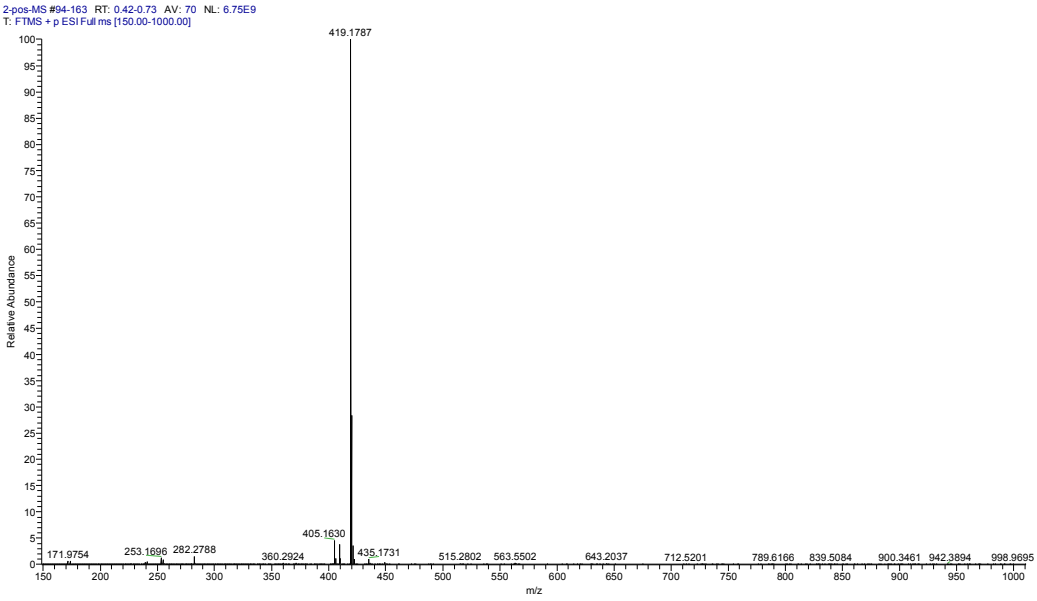

Figure S23. HRMS chart of **SO_2R4**.

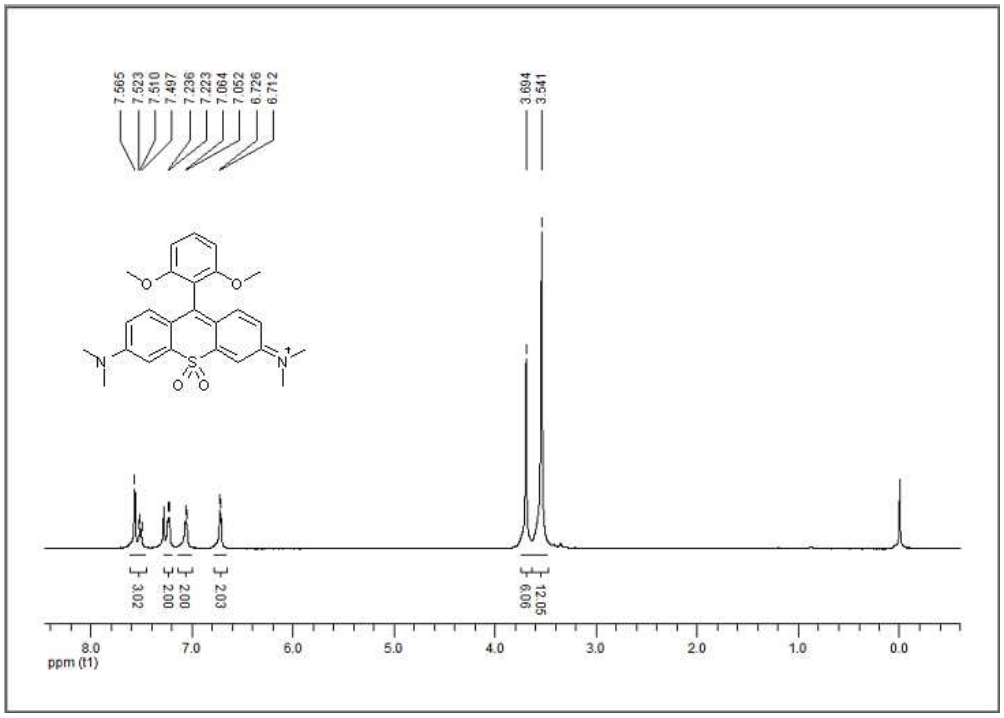

Figure S24. ^{1}H NMR chart of **SO_2R5** ($CDCl_3$, 600 MHz).

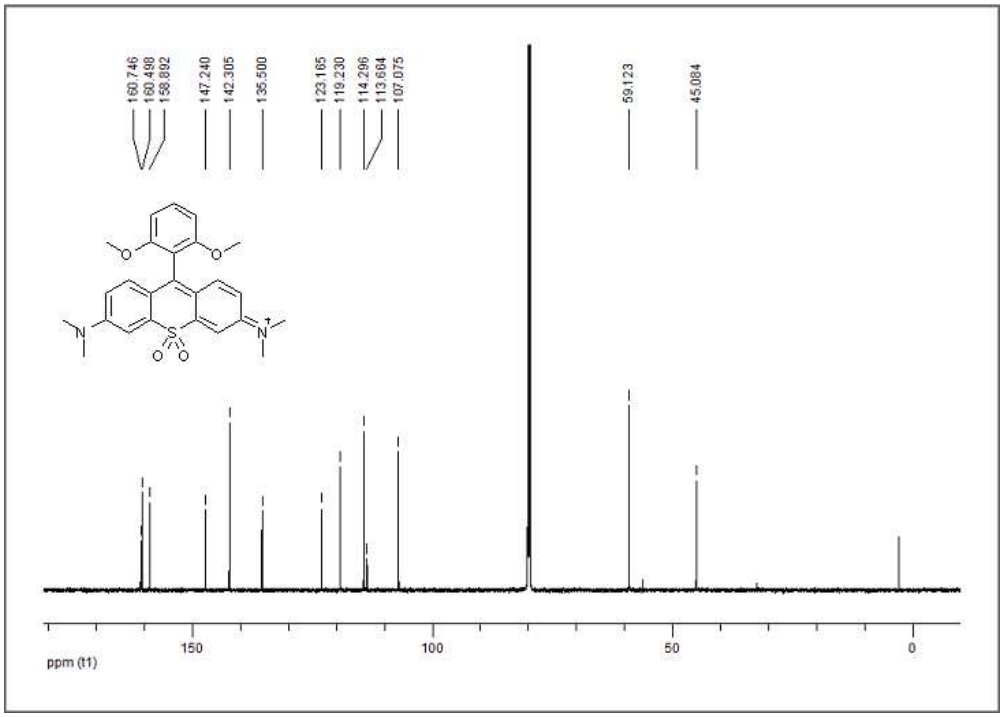

Figure S25. ^{13}C NMR chart of **SO_2R5** ($CDCl_3$, 150 MHz).

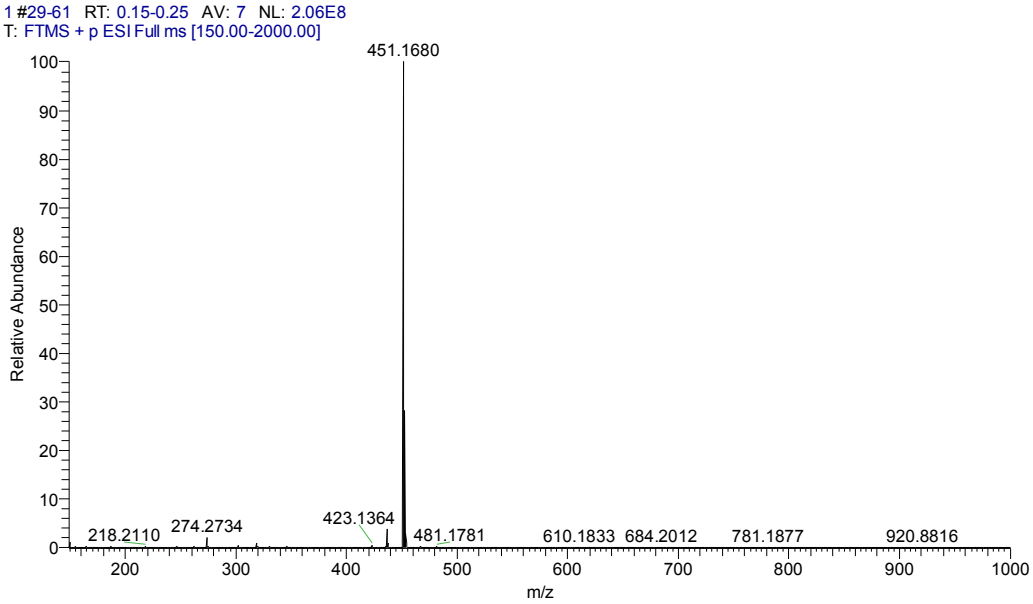

Figure S26. HRMS chart of **SO_2R5**.

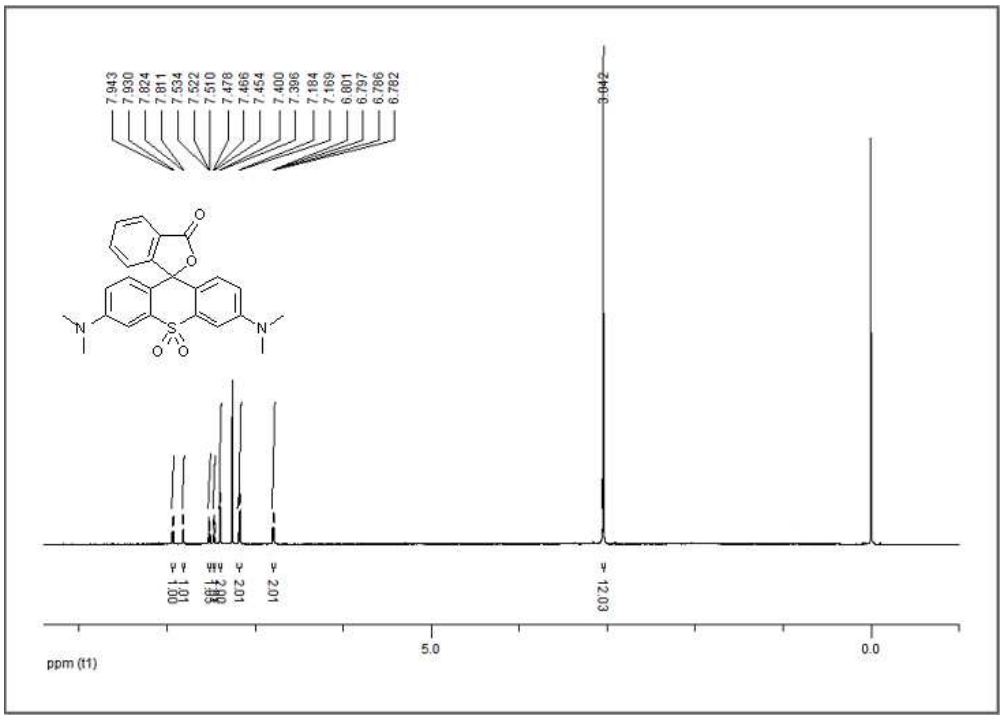

Figure S27. ^{1}H NMR chart of **SO_2R6** ($CDCl_3$, 600 MHz).

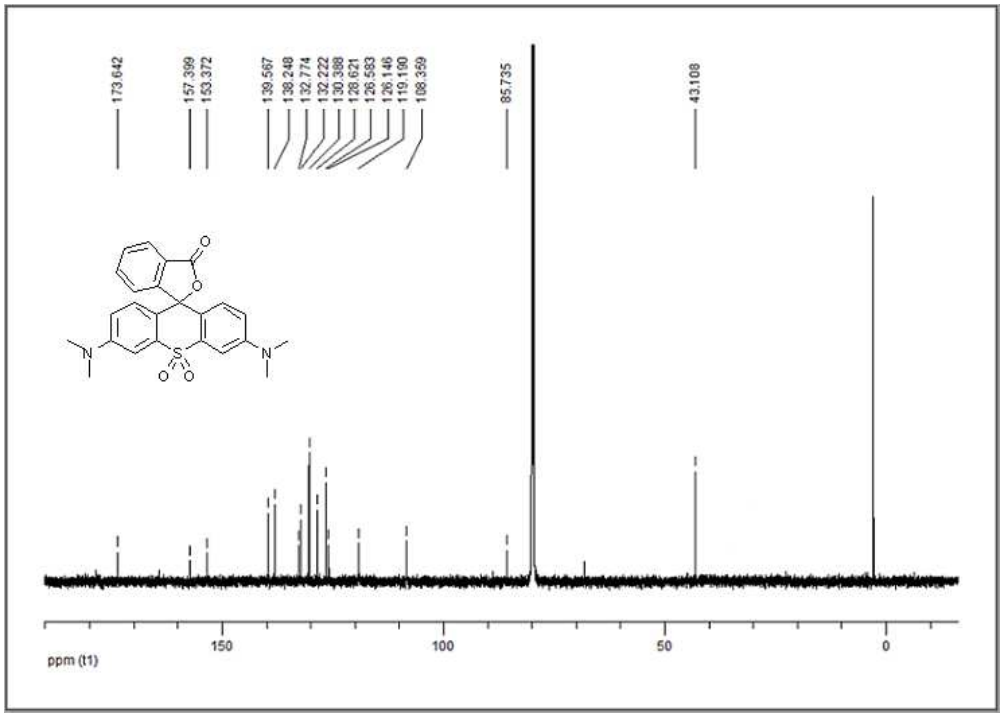

Figure S28. ^{13}C NMR chart of **SO_2R6** ($CDCl_3$, 150 MHz).

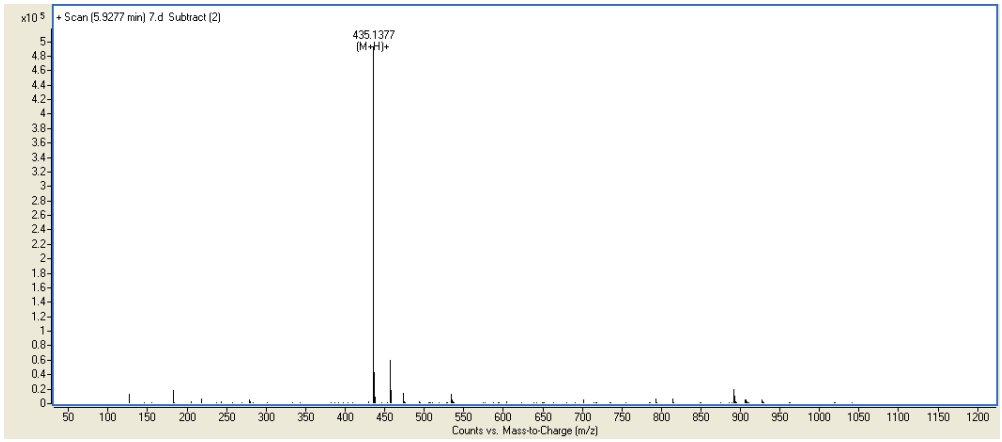

Figure S29. HRMS chart of **SO_2R6**.

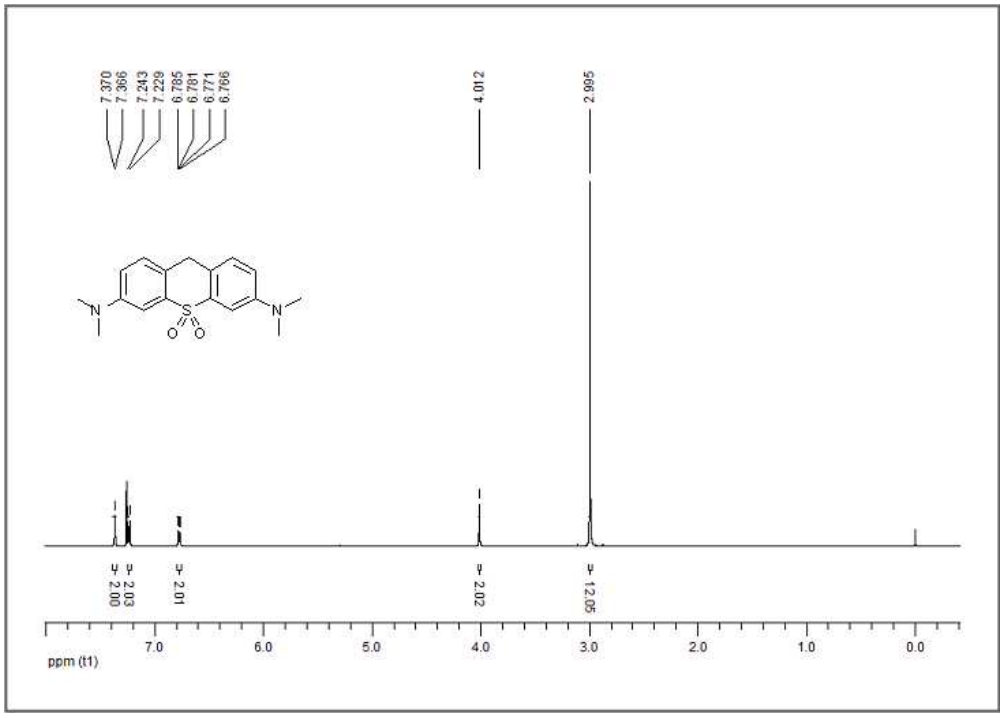

Figure S30. ^{1}H NMR chart of compound **2** ($CDCl_3$, 600 MHz).

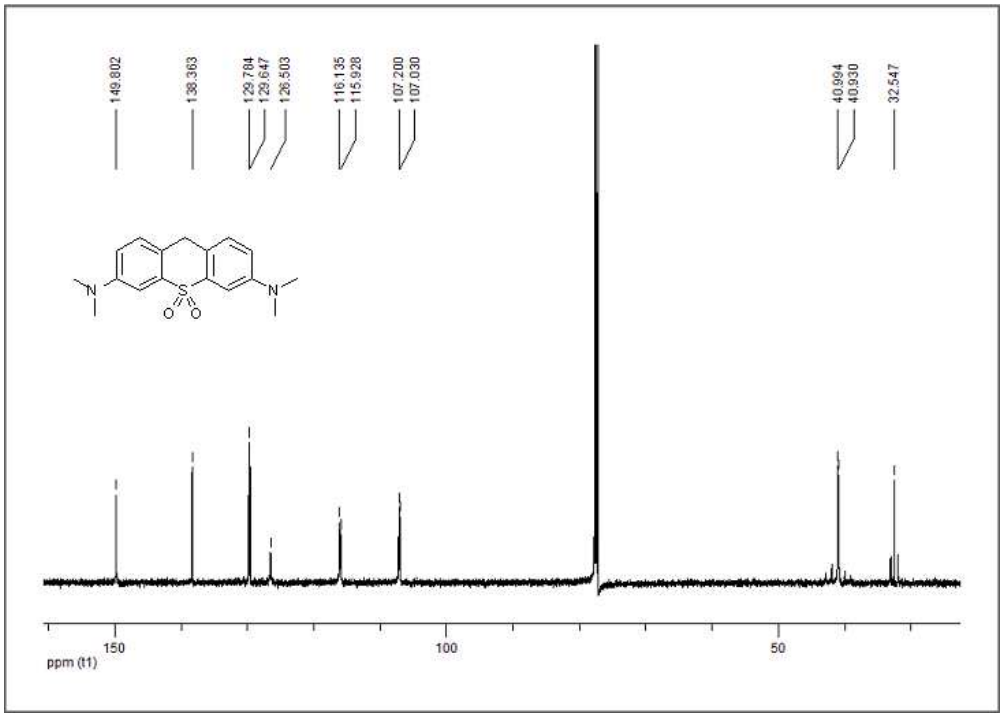

Figure S31. ^{13}C NMR chart of compound **2** ($CDCl_3$, 150 MHz).

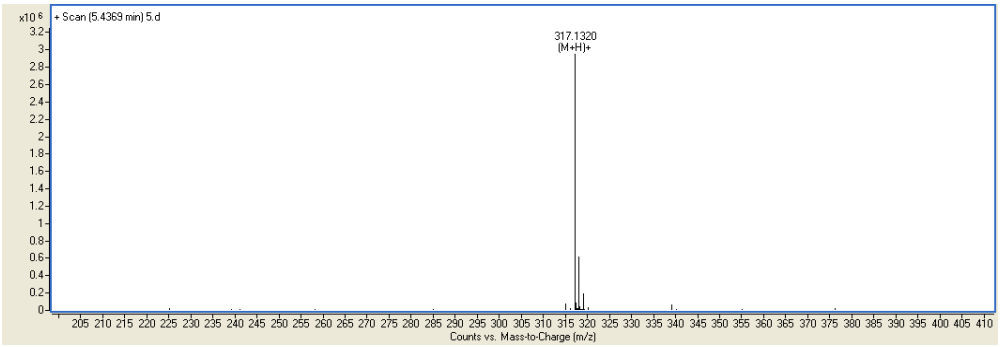

Figure S32. HRMS chart of compound **2**.

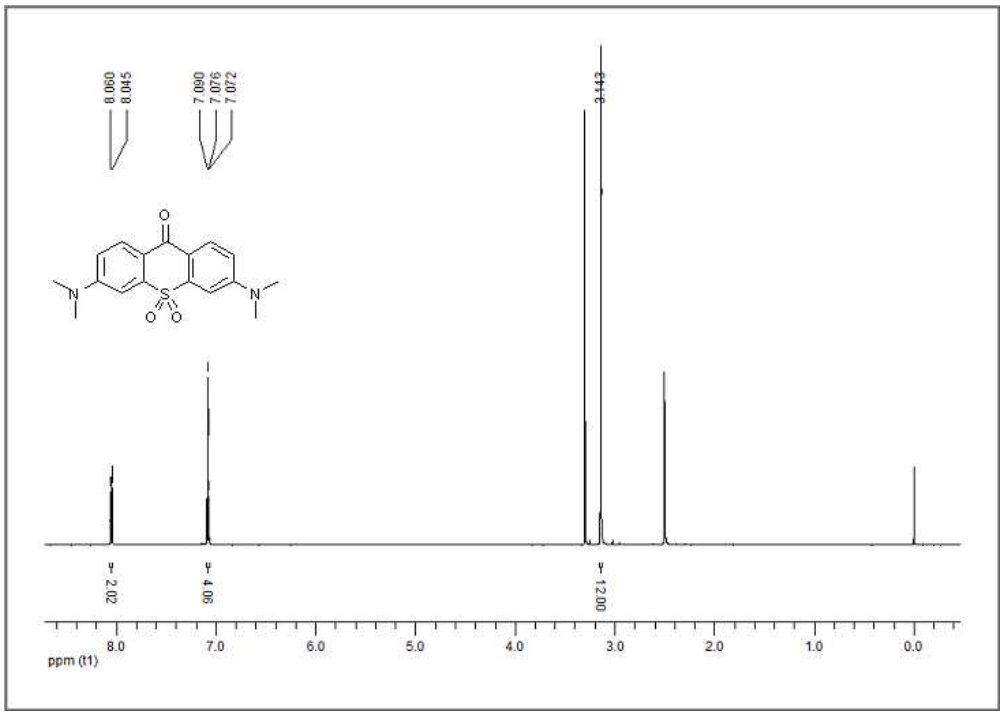

Figure S33. ^{1}H NMR chart of compound **3** (DMSO-d_6, 600 MHz).

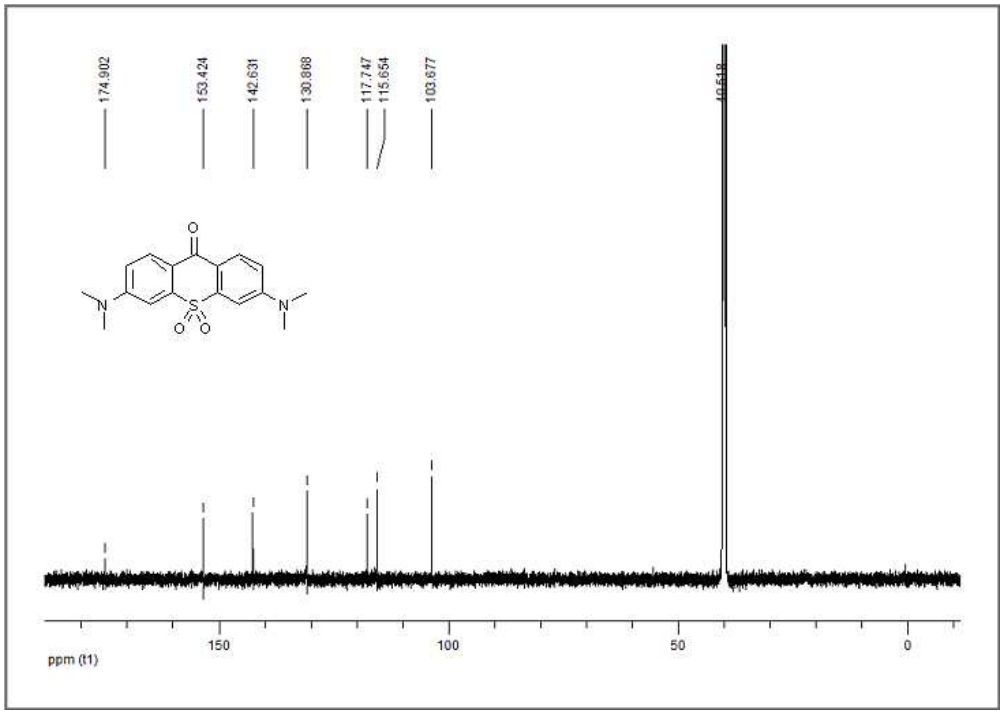

Figure S34. ^{13}C NMR chart of compound **3** (DMSO-d_6, 150 MHz).

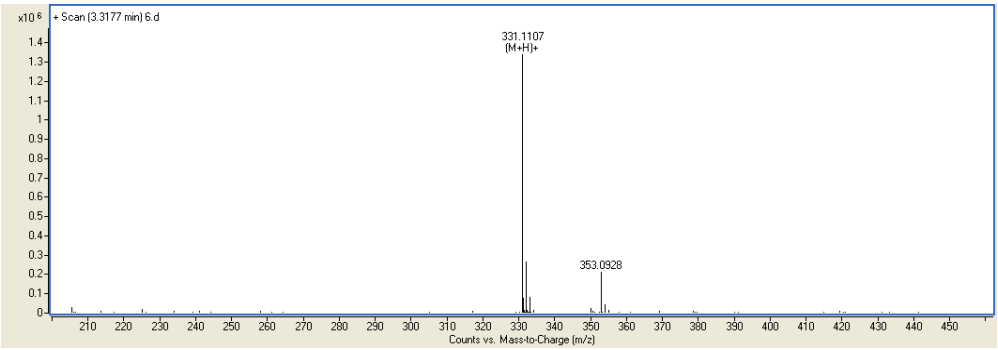

Figure S35. HRMS chart of compound **3**.

3. References

(1) Poole, B.; Ohkuma, S. *J. Cell Biol.*, **1981**, *90*, 665–669.

(2) Zhang, X.; Wang, C.; Han, Z.; Xiao, Y. *ACS Appl. Mater. Interfaces*, **2014**, *6*, 21669–21676.